npj | wireless technology

Article

https://doi.org/10.1038/s44459-026-00055-w

A&M based fractional delay and Doppler channel estimation in OTFS

Check for updates

Omid Abbassi Aghda[1,2] ✉, Oussama Ben Haj Belkacem[1,3], Nikolajs Tihomorskis[4], João Guerreiro[1,2], Nuno Souto[1,5], Michal Szczachor[6] & Rui Dinis[1,2]

Orthogonal time frequency space (OTFS) modulation is a candidate for low-density high-mobility communication (LDHMC) use case in sixth generation (6G) due to its robustness against Doppler effects. This paper presents a low-complexity channel estimation method based on the A&M frequency estimation algorithm, enabling precise recovery of fractional delay, Doppler, and gain. We show that conventional virtual tap-based methods are inadequate for detection, while sparse Bayesian learning (SBL)-based off-grid approaches, though precise, are computationally intensive. To bridge this gap, we propose a method that combines precision with efficiency, eliminating the trade-off between accuracy and complexity. Its effectiveness is validated through MATLAB simulations and real-time implementation on an Ettus USRP B210 SDR platform.

The use cases defined in fifth generation (5G) mobile network include enhanced mobile broadband (eMBB), ultra-reliable low-latency communications (URLLC), and massive machine-type communications (mMTC). In the context of sixth generation (6G) mobile network, these use cases need to be further enhanced. This leads to further enhanced mobile broadband (feMBB), enhanced ultra-reliable low-latency communications (eURLLC), and ultra-massive machine-type communications (umMTC). In addition to these, two new use cases are introduced: long-distance and high-mobility communications (LDHMC) and enhanced low-power communications (eLPC). These latter two require new investigations to design systems capable of supporting such advanced scenarios[1,2]. Specifically, LDHMC in 6g may involve applications that exceed the current maximum mobility expectations of 500 km/h, potentially requiring communication capabilities at speeds up to 1000 km/h. This includes emerging domains such as deep-sea tourism, space tourism, and ultra-high-speed rail systems[3].

Orthogonal time frequency space (OTFS) modulation, proposed in ref. 4, is a strong candidate for high-speed environments due to its demonstrated ability to handle doubly dispersive channels. In this modulation, information symbols are mapped in the delay-Doppler (DD) domain, where the channel is treated as time-invariant, even though it is inherently time-variant, making the system robust to extreme mobility conditions. At the receiver, the transmitted symbols are coupled with the DD channel through a 2D phase-shifted convolution, which enables reliable performance even at very high speeds[5]. Since its proposal in 2017, extensive research has been conducted on the system design of OTFS. One prominent research direction is led by the authors of ref. 6, who analyzed the complete OTFS system, including channel modeling, data detection, and channel estimation, and compared it with orthogonal frequency-division multiplexing (OFDM) modulation. As system performance heavily depends on accurate channel estimation, this paper focuses on the channel estimation aspect.

In ref. 7, the authors proposed an impulse-based channel estimation method where a single sample is multiplexed across the entire DD domain. At the receiver, a threshold-based algorithm detects the location and coefficients of channel taps, revealing delay and Doppler shifts. Although the method extends to multiple-input multiple-output (MIMO) systems, it does not account for fractional delay and Doppler, which arise when normalized delay and Doppler values misalign with the sampled DD grid. To address fractional Doppler and reduce pilot overhead, Raviteja et al.[8] introduced an embedded pilot (EP)-based technique. Pilot and data symbols are transmitted within the same frame, separated by zero-valued guard intervals to prevent interference. This design reduces overhead and models fractional Doppler as virtual taps, enabling low-complexity estimation with good performance. However, data detection using the estimated channel yields poor performance, a limitation examined in this paper. Other works, such as refs. 9,10, employ sparse recovery algorithms to exploit channel sparsity in the DD domain. Nevertheless, these methods still rely on capturing virtual taps rather than estimating the actual delay and Doppler values. The authors of ref. 11 proposed the variable resolution coarse-to-fine (VRCF) method to estimate fractional Doppler. Their method is based on a channel model with integer delays, where each delay bin contains multiple taps with different fractional Doppler shifts. The VRCF method consists of a coarse and a fine estimation stage. In the coarse stage, integer Doppler is estimated using integer sampling points, followed by higher-resolution sampling to approximate fractional Doppler. The fine stage applies iterative interference

[1]Instituto de Telecomunicações, Lisbon, Portugal. [2]Universidade Nova de Lisboa, Monte da Caparica, Portugal. [3]Innov'Com Laboratory, orgnameSup'Com, University of Carthage, Tunis, Tunisia. [4]Institute of Photonics, Electronics and Telecommunications, Riga Technical University, Riga, Latvia. [5]ISCTE-Instituto Universitário de Lisboa, Lisbon, Portugal. [6]Nokia, Wroclaw, Wrocław, Poland. ✉e-mail: o.aghda@campus.fct.unl.pt

cancellation to mitigate inter-Doppler interference (IDI), using a fixed-resolution module followed by a variable-resolution module to balance performance and complexity. Despite its effectiveness, the overall complexity of the VRCF method is high, and it assumes prior knowledge of the number of channel taps per delay at the receiver. The aforementioned methods that focus solely on the fractional Doppler issue typically operate under the condition that the bandwidth is sufficiently large and that the channel exhibits fractional Doppler and integer delay only. However, when the data rate per frame is fixed, addressing fractional Doppler inherently challenges the assumption that delay values are integers[12]. Therefore, it is important to jointly consider fractional delay and Doppler.

To simultaneously address fractional delay and Doppler, off-grid methods have also been explored. These approaches aim to estimate the exact values of delay and Doppler rather than relying on a discretized grid. Leveraging the sparse nature of the DD domain, off-grid sparse recovery techniques have been proposed to improve estimation accuracy. In ref. 13, the authors introduced the grid refinement and adjustment-based sparse Bayesian inference (GRASBI) method for channel parameter estimation in orthogonal delay-Doppler division multiplexing (ODDM) systems. The approach begins by estimating channel parameters, gain, delay, and Doppler, using a dense virtual grid and the sparse Bayesian learning (SBL) algorithm. A grid refinement step then creates a denser grid around the initially estimated tap locations. Subsequently, a grid adjustment procedure, guided by a maximum likelihood (ML) criterion, iteratively minimizes the mismatch between the actual tap positions and the adjusted grid. To reduce computational complexity, the authors proposed grid refinement and adjustment-based sparse Bayesian inference with Student's t distribution (TGRAESBI), which simplifies the SBL step by replacing full matrix inversion with diagonal matrix inversion. The proposed method outperforms other off-grid DD channel estimation techniques, such as off-grid sparse Bayesian inference (OGSBI)[14], grid evolution-based sparse Bayesian inference (GESBI)[15], and grid evolution-based efficient sparse Bayesian inference with Student's t distribution (T-GEESBI)[16], while maintaining comparable complexity to GESBI and T-GEESBI. Its advantage over OGSBI lies in avoiding approximation, and its superiority over GESBI and T-GEESBI stems from the iterative use of grid refinement and adjustment in the SBL estimation process. Despite its improved performance, GRASBI still suffers from high computational complexity, typical of SBL-based off-grid methods. Moreover, while it achieves accurate Doppler estimation for each tap, its delay estimation performance remains limited. Motivated by the high complexity of SBL-based off-grid estimation, this paper proposes a low-complexity method with strong performance in both delay and Doppler domains.

Other studies have proposed methods for estimating fractional delay and Doppler in radar and integrated sensing and communication (ISAC) applications. In ref. 17, the authors used time-frequency (TF) spreading codes, previously applied in Gabor division spread spectrum (GDSS) systems, to approximate the ambiguity function of the GDSS signal as a 2D sinc function. They proposed two algorithms: the first uses 2D sinc interpolation via optimization for higher accuracy, while the second employs quadratic interpolation to provide an approximate closed-form solution that can serve as an initial point for the first algorithm. The approach presented in the paper offers a good trade-off between complexity and performance. However, it is limited to radar scenarios with a single tap and does not address multi-tap channels. Additionally, it lacks comparison with other methods and only evaluates the root mean square error (RMSE) of the two proposed algorithms. In ref. 18, the authors prove that the range-velocity (RV) matrix used in conventional radar sensing is equivalent to the DD channel representation. They further demonstrate an equivalence between the fast time-slow-time (FTST) and delay-time (DT) matrices, which supports the relevance of OTFS in ISAC system. Based on this, the authors proposed an approximate closed-form solution for estimating fractional delay and Doppler using pulse compression and 2D correlation between the received and transmitted signals in the DD domain. However, this method is only applicable when no two-channel taps share the same integer delay or Doppler. In ref. 19, a 2D correlation-based framework was used to propose the maximum likelihood based on multi-frame superposition (ML-MFS) method for estimating channel parameters, including fractional delay and Doppler, in ISAC applications. This method improves performance with lower complexity compared to ref. 20, which applies ML after 2D correlation. To further enhance performance, the authors introduced whale optimization multi-frame superposition (WOA-MFS). However, the method assumes channel parameters remain constant over a super-frame, which may not hold in high-Doppler scenarios. Moreover, its reliance on multiple frames makes it unsuitable for delay-sensitive applications that require rapid symbol detection. Inspired by these works, we aim to develop a delay and Doppler estimation algorithm that not only maintains low complexity but also performs effectively in line-of-sight (LoS) scenarios, making it suitable for ISAC applications and object tracking.

The proposed channel estimation method draws inspiration from the classical frequency estimation problem, motivating a brief review of interpolation-based techniques commonly used for frequency estimation. In ref. 21, the authors proposed the Aboutanios and Mulgrew (A&M) method, an iterative, low-complexity frequency estimation technique based on evaluating the discrete time Fourier transform (DTFT) at offsets of ±0.5 frequency bins around the peak index of the discrete Fourier transform (DFT). They derived analytical performance bounds and showed that the method asymptotically achieves the Cramer-Rao lower bound (CRLB) across the entire frequency range. It was demonstrated that only two iterations are sufficient for good performance, and additional iterations offer no significant improvement. In ref. 22, the authors introduced the q-shift estimator (QSE) and hybrid A&M and q-shift estimator (HAQSE) methods. The QSE method evaluates the DTFT in the vicinity of the DFT peak using q-shifted samples, iteratively refining the frequency estimate. It was shown to be asymptotically unbiased, with optimal performance achieved in just three iterations, including the determination of the optimal q value. To reduce complexity to two iterations, the HAQSE method was proposed. In its first iteration, it employs the A&M interpolator from refs. 21,23. HAQSE also performs better when the number of samples is small, due to the lower bias of the A&M interpolator in the initial iteration. In ref. 24, a low-complexity yet efficient method was proposed to estimate multiple frequency components. This method, named coarse-to-fine HAQSE (CFH), builds upon HAQSE and applies it iteratively. Simulation results show that although CFH has a higher signal-to-noise ratio (SNR) threshold, it eventually reaches the CRLB and outperforms other methods such as multiple signal classification (MUSIC), estimation of signal parameters via rotational invariance techniques (ESPRIT), and the RELAX algorithm. In ref. 25, the authors proposed a 2D frequency estimation method for complex exponential signals, later extended to the k-dimensional (kD) case. The method is based on QSE from ref. 22, and to improve coarse estimation and enhance the SNR breakdown threshold, they introduced the QSE method, which utilizes two-stage interpolation.

Existing methods, such as refs. 7–10, often rely on virtual taps to capture fractional delay and Doppler effects, which can degrade symbol detection performance. We analyze this limitation and explain why virtual tap-based estimation fails to provide reliable data detection. Other approaches, such as SBL-based off-grid techniques in refs. 13–16, offer high accuracy but suffer from high computational cost and restrictive assumptions, such as requiring unique integer delays or Doppler values[18], or assuming channel parameters remain constant over long frames[19]. To address these issues, we propose a novel channel estimation algorithm inspired by the A&M frequency estimation technique and the 2D HAQSE framework. Our contribution includes

- Revealing that fractional delay and Doppler estimation in OTFS can be reformulated as a frequency-estimation problem, which opens the door to applying a broad class of existing frequency-estimation techniques to OTFS channel estimation.
- Applying a sinc-based approximation and a phase compensation coefficient to adapt the fractional delay model for compatibility with

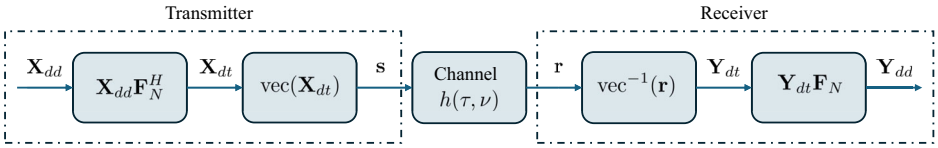


Fig. 1 | Block diagram of the OTFS transceiver. The transmitter maps the DD domain input matrix $\mathbf{X}_{dd}$ to the dt domain using an IDFT along rows, followed by column-wise vectorization to generate the transmit signal **s**, which propagates through a DD channel. At the receiver, the received signal **r** is reshaped to obtain $\mathbf{Y}_{dt}$, and a DFT is applied to recover the DD domain output matrix $\mathbf{Y}_{dd}$. Dashed boxes denote transmitter and receiver processing blocks. The figure was generated using Microsoft PowerPoint.

the A&M algorithm. We then apply the A&M algorithm to the 2D scenario to estimate fractional delay and Doppler, inspired by the 2D HAQSE framework.

- Analyzing the shortcomings of virtual tap-based estimation in the context of data detection, and demonstrating its impact on performance using bit error rate (BER) curves presented in the Results section.
- Achieving lower estimation error than both conventional EP and SBL-based approaches, while maintaining low computational complexity.
- Evaluating the method under both LoS and non line of sight (NLoS) scenario. For the LOS case, we validate its performance using a real-time software-defined radio (SDR) setup with an Ettus USRP B210.

The remainder of this paper is organized as follows. The Methods section describes the system model and formulates the problem, highlighting the importance of estimating fractional delay and Doppler components. It also presents the proposed channel estimation approach, addressing both LoS and NLoS scenarios, along with an analysis of computational complexity. The Results section reports simulation outcomes that validate the effectiveness of the proposed method, including MATLAB and SDR-based implementations. Finally, the Discussion section summarizes the key findings and their practical implications.

Notation

Lowercase normal letters, bold lowercase letters, and bold uppercase letters represent scalars, vectors, and matrices, respectively. The notation $r(t)$ refers to a continuous-time scalar signal evaluated at $t \in \mathbb{R}$, while $\mathbf{r}[n]$ denotes the nth discrete-time sample at $n \in \mathbb{Z}$ of the vector **r**. Similarly, $\mathbf{X}[m, n]$ represents the element at the mth row and nth column of the matrix **X**. Additionally, $\mathbf{X}[m,:]$ and $\mathbf{X}[:, n]$ denote the selection of the mth row and nth column of the matrix **X**, respectively. The operations $(.)^H$, $(.)^T$, and vec(.) denote the Hermitian transpose, transpose, and column-wise vectorization, respectively. The notation $(.)_M$ indicates the modulo-M operation applied to the argument. $\Re\{\cdot\}$ denotes the real part of a complex number.

Methods

The structure of this section is as follows. The System Model subsection presents the system model, which includes the transmitter, receiver, and the input-output relationship in the OTFS modulation framework. This part also discusses the channel model and emphasizes the importance of estimating fractional delay and Doppler components. The Channel Estimation - LOS Scenario subsection introduces the proposed channel estimation method for the LoS case, where the estimation of channel parameters (delay, Doppler shift, and channel gain) is detailed. The Channel Estimation-NLOS Scenario subsection generalizes the approach to the NLoS scenario. Finally, the Computational Complexity subsection provides an analysis of the computational complexity of the proposed method.

System model

In OTFS modulation, information symbols are multiplexed in the DD domain, represented by the matrix $\mathbf{X}_{\mathrm{dd}} \in \mathbb{C}^{M\times N}$. This matrix captures the sampled DD domain, where the sampling intervals along the delay and Doppler axes are given by $\frac{1}{M\Delta f}$ and $\frac{1}{NT}$, respectively. Here, M and N denote the number of bins along the delay and Doppler axes, respectively. The subcarrier spacing in the equivalent TF domain is defined as $\Delta f = \frac{1}{T}$, where T is the duration of one OTFS subsymbol. Consequently, the total bandwidth is $B = M\Delta f$ and the duration of one OTFS symbol is $T_f = NT$[6]. Figure 1 illustrates the transceiver system model of the OTFS modulation scheme.

To generate the time-domain signal, we first apply the inverse discrete Fourier transform (IDFT) along the Doppler axis (rows of $\mathbf{X}_{\mathrm{dd}}$), resulting in the DT domain representation of the signal. This transformation is expressed as

$$\mathbf{X}_{\mathrm{dt}} = \mathbf{X}_{\mathrm{dd}}\,\mathbf{F}_N^H \in \mathbb{C}^{M\times N}, \tag{1}$$

where $\mathbf{F}_N \in \mathbb{C}^{N\times N}$ is the DFT matrix. The time-domain signal is then obtained by vectorizing $\mathbf{X}_{\mathrm{dt}}$ along the columns

$$\mathbf{s} = \mathrm{vec}\left(\mathbf{X}_{\mathrm{dt}}\right) \in \mathbb{C}^{MN\times 1}. \tag{2}$$

Finally, a cyclic prefix (CP) of minimum length equal to the maximum delay spread of the channel is appended to **s**, resulting in the discrete transmitted signal $\mathbf{s}_{\mathrm{cp}}$[6], whose continuous-time representation is denoted by $s_{\mathrm{cp}}(t)$.

The continuous signal $s_{\mathrm{cp}}(t)$ is transmitted through a high-mobility wireless channel, which can be represented in the DD domain as

$$h(\tau,\nu) = \sum_{i=1}^{P} h_i \delta(\tau-\tau_i, \nu-\nu_i), \tag{3}$$

where P is the number of propagation paths, and h_i, τ_i, and ν_i denote the complex gain, delay, and Doppler shift of the i^{th} path, respectively. The normalized delay and Doppler indices for each path are given by

$$l_i = \tau_i\, M\,\Delta f = \tau_i B = l_{il} + l_{iF},\; k_i = \nu_i\, N\, T = \nu_i\, T_f = k_{il} + k_{iF},$$

where $l_{il} \in \mathbb{Z} \cap [0, l_{\max}]$ and $k_{il} \in \mathbb{Z} \cap [-k_{\max}, k_{\max}]$ are the integer parts, and $l_{iF}, k_{iF} \in [-0.5, 0.5]$ are the fractional parts of the normalized delay and Doppler indices, respectively. Here, $l_{\max}$ and $k_{\max}$ denote the maximum normalized delay and Doppler spread of the channel.

The continuous-time received signal can be expressed as[6]

$$r(t) = \sum_{i=1}^{P} h_i e^{j2\pi\nu_i(t-\tau_i)} s_{\mathrm{cp}}(t-\tau_i). \tag{4}$$

To express $s_{\mathrm{cp}}(t)$ in terms of its discrete samples, we apply the Whittaker-Shannon interpolation formula. This yields the continuous-time received signal as[26]

$$r(t) = \sum_{i=1}^{P} h_i e^{j2\pi\nu_i(t-\tau_i)} \sum_{q'=-\infty}^{\infty} \mathbf{s}_{\mathrm{cp}}[q']\,\mathrm{sinc}\left(Bt - B\tau_i - q'\right). \tag{5}$$

Sampling the received signal at rate B, i.e., at $t = \frac{q}{B}, q = 0, \ldots, MN-1$, and removing CP gives the discrete-time

received signal

$$\mathbf{r}[q] = r\left(\frac{q}{B}\right) = \sum_{q'=-\infty}^{\infty} \mathbf{s}\left[(q-q')_{MN}\right] \sum_{i=1}^{P} h_i e^{j2\pi \frac{k_i(q-l_i)}{MN}} \operatorname{sinc}(q'-l_i); q = 0, \ldots, MN-1. \tag{6}$$

The circular shift in (6) is the effect of CP. Based on (6), the time-varying channel impulse response at time index q is defined as

$$\mathbf{g}_q[q'] = \sum_{i=1}^{P} h_i\, e^{j2\pi \frac{k_i(q-l_i)}{MN}} \operatorname{sinc}(q'-l_i); q' \in \mathbb{Z}. \tag{7}$$

Assuming the system is causal and the channel response is negligible for effective delays beyond M (i.e., $g_q[q'] = 0$ for $q' \geq M, q' < 0$), the received signal simplifies to

$$\mathbf{r}[q] = \sum_{q'=0}^{M-1} \mathbf{s}[(q-q')_{MN}]\, \mathbf{g}_q[q']. \tag{8}$$

This represents a time-varying circular convolution between the transmitted signal and the effective channel impulse response. Notably, the effective channel experienced by the transmitted samples may exhibit a delay spread larger than the maximum physical delay $l_{\max}$, due to the fractional delay effect introduced by the sinc interpolation.

At the receiver, the time-domain received vector $\mathbf{r} \in \mathbb{C}^{MN\times 1}$, composed of elements $\mathbf{r}[q]$, is reshaped via unvectorization to obtain the DT domain representation of the received signal as

$$\mathbf{Y}_{\mathrm{dt}} = \mathrm{vec}^{-1}(\mathbf{r}) \in \mathbb{C}^{M\times N}. \tag{9}$$

To recover the DD domain representation, a DFT is applied along the time axis (i.e., across the rows of $\mathbf{Y}_{\mathrm{dt}}$)

$$\mathbf{Y}_{\mathrm{dd}} = \mathbf{Y}_{\mathrm{dt}}\, \mathbf{F}_N \in \mathbb{C}^{M\times N}. \tag{10}$$

The relationship between the elements of the received DD domain signal matrix $\mathbf{Y}_{\mathrm{dd}}$ and the transmitted matrix $\mathbf{X}_{\mathrm{dd}}$ is governed by a 2D phase-shifted convolution. This convolution operates between the transmitted signal symbols and the effective DD domain channel response and is expressed as

$$\begin{aligned}\mathbf{Y}_{\mathrm{dd}}[m,n] &= \sum_{m'=0}^{M-1}\sum_{n'=0}^{N-1} \mathbf{h}_{m,n}[m',n']\, \mathbf{X}_{\mathrm{dd}}[(m-m')_M, (n-n')_N] \\ &= \frac{1}{N}\sum_{i=1}^{P}\sum_{m'=0}^{M-1}\sum_{n'=0}^{N-1} h_{i,m-m'}\, \alpha_i(m,m',n,n') \\ &\quad \times \zeta_N(k_i-n')\, \operatorname{sinc}(m'-l_i)\, \mathbf{X}_{\mathrm{dd}}[(m-m')_M, (n-n')_N].\end{aligned} \tag{11}$$

The term $h_{i,m-m'} = h_i\, e^{j2\pi \frac{k_i(m-m')}{MN}}$ represents the phase-shifted channel coefficient and $\mathbf{h}_{m,n}[m',n']$ in (11) represents the effective DD domain channel response and is defined as

$$\mathbf{h}_{m,n}[m',n'] = \sum_{i=1}^{P} h_{i,m-m'}\, \alpha_i(m,m',n,n')\, \zeta_N(k_i-n')\, \operatorname{sinc}(m'-l_i). \tag{12}$$

The periodic phase shifted sinc function $\zeta_N(x)$, which arises due to fractional Doppler, is defined as

$$\zeta_N(x) = \frac{\sin(\pi x)}{\sin(\pi x/N)}\, e^{j\pi x(N-1)/N}. \tag{13}$$

The function $\alpha_i(m,m',n,n')$ accounts for the phase discontinuity caused by circular delay wrapping and is given by

$$\alpha_i(m,m',n,n') = \begin{cases} 1, & \text{if } m' \leq m < M, \\ e^{-j2\pi \frac{(n-n')_N}{N}}, & \text{otherwise}. \end{cases} \tag{14}$$

Examining the input-output relationship in (11), we observe that the received symbol at the (m, n)th DD bin is a weighted sum of transmitted symbols at positions $(m-m', n-n')$, each modulated by a complex gain. This gain includes a phase term $e^{j2\pi \frac{k_i(m-m')}{MN}}$, which depends on the true Doppler shift k_i and the delay index offset $(m-m')$. This phase shift varies with the delay position of the transmitted symbol, making the received signal sensitive to true Doppler value and delay index of transmitted symbol. One might consider estimating the effective channel taps directly in the DD domain using pilot symbols[8–10]. However, due to the phase shift dependency on both the delay of the transmitted pilot and the true Doppler value, the estimated effective gain does not generalize well across different delay indices. As a result, this estimate cannot be directly reused for data symbols located at other delay positions, since they experience different phase rotations.

Therefore, accurate estimation of the true physical delay and Doppler parameters is essential, not only to capture the correct channel behavior and reduce detection complexity, but also to improve overall detection performance. Relying solely on virtual channel taps (resulting from sinc interpolation) leads to a dense channel representation, which significantly increases the complexity of symbol detection.

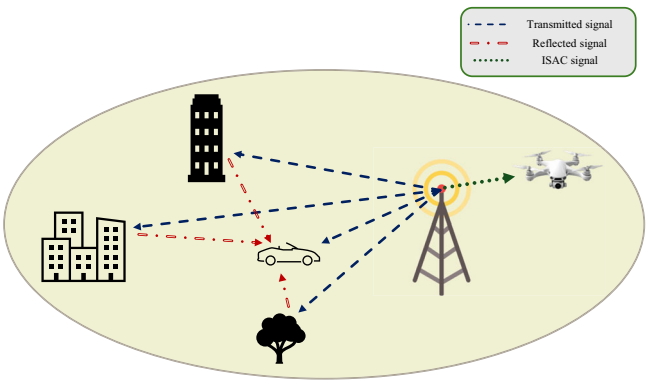


Fig. 2 | LOS and NLOS scenarios in an OTFS-based ISAC environment. In the LOS case, a base station directly transmits a signal toward a UAV, shown with a dotted green line. In the NLOS case, a receiver inside a vehicle is surrounded by reflecting objects, resulting in multipath propagation. The transmitted signal toward the vehicle and surrounding buildings is shown with a dashed blue line, while the reflected signal toward the vehicle is shown with a dashed red line. The shaded region indicates the system coverage area. The figure was generated using Microsoft PowerPoint. Icon made by Freepik from www.flaticon.com.

Channel estimation - LOS scenario

We begin by focusing on the LoS channel model, which offers a clearer understanding of the A&M algorithm and serves as a foundation for extending the method to more complex environments. As illustrated in Fig. 2, this model supports ISAC applications, enabling unmanned aerial vehicle (UAV)s to extract spatial information from the channel in the DD domain, analogous to the range-velocity domain in radar systems. The figure also depicts an NLoS scenario, such as the case where a receiver inside a car operates in a rich multipath environment. The generalization to the NLoS case, involving multiple taps, is discussed in subsection Channel Estimation - NLOS Scenario

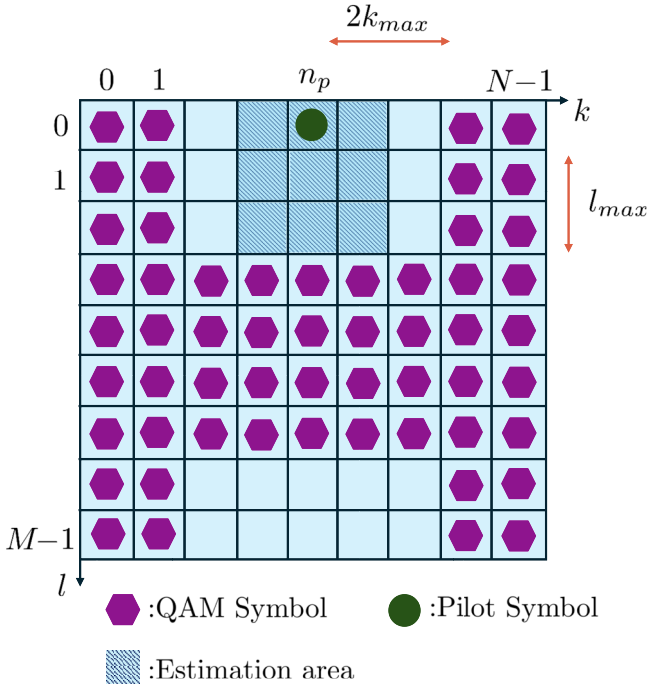


Fig. 3 | QAM and pilot symbol placement in the DD domain. The pilot symbol is indicated with a green circle, while QAM symbols are represented with purple hexagons. The hatched region denotes the receiver observations used for channel estimation. The pilot is placed at delay index $m_p = 0$ to eliminate the phase shift introduced in Eq. (14), which also reduces the dependency of channel gain estimation on Doppler accuracy, as discussed in System Model. The figure was generated using Microsoft PowerPoint.

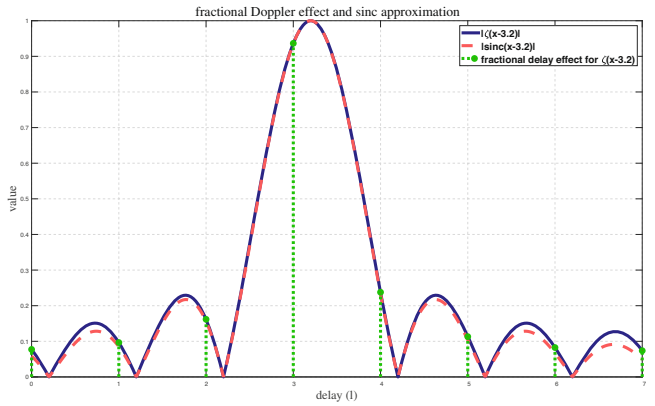


Fig. 4 | Effect of fractional delay with delay set to 3.2 and integer Doppler. The dashed red line shows $|\mathrm{sinc}(x-3.2)|$, while the solid blue line represents $|\zeta(x-3.2)|$. Sample values at integer delays from the sinc function are indicated with a dotted green line. The figure highlights that $\zeta(x)$ closely approximates the sinc function near the peak, where most of the signal power is concentrated, while minor deviations away from the peak have negligible impact. The figure was generated using MATLAB.

We estimate the channel parameters under the assumption of a single tap, characterized by a normalized delay $l_{\mathrm{LoS}} = l_{\mathrm{LoS},I} + l_{\mathrm{LoS},F}$, a normalized Doppler shift $k_{\mathrm{LoS}} = k_{\mathrm{LoS},I} + k_{\mathrm{LoS},F}$, and a channel gain h_{LoS}. Here, the subscripts I and F indicate the integer and fractional parts of the channel parameters, respectively. We begin by presenting the problem setup, followed by an overview of the frequency estimation problem and its connection to DD channel estimation. Subsequently, we detail the estimation procedures for Doppler, delay, and channel gain.

We consider an impulse-based pilot defined as

$$\mathbf{X}_{\mathrm{dd}}[m,n] = \begin{cases} x_p, & (m,n) = (m_p, n_p) \\ 0, & m \in \mathcal{P}_m,\ n \in \mathcal{P}_n,\ (m,n) \neq (m_p, n_p) \\ x_d[m,n], & \text{otherwise} \end{cases} \tag{15}$$

where x_p is the impulse value, and (m_p, n_p) denotes its location in the DD domain. The index sets for the pilot guard are defined as

$$\mathcal{P}_m = \left[(m_p - l_{\max})_M, (m_p + l_{\max})_M\right],\ \mathcal{P}_n = \left[(n_p - 2k_{\max})_N, (n_p + 2k_{\max})_N\right].$$

Refer to Fig. 3, which shows the arrangement of quadrature amplitude modulation (QAM) and pilot symbol in the DD domain. We place the pilot symbol at delay index $m_p = 0$ to eliminate the additional phase shift introduced in Eq. (14). This choice also reduces the dependency of channel gain estimation on the accuracy of Doppler estimation, as discussed in System Model. The shaded area in the figure indicates the region of samples used at the receiver to estimate the channel. This region spans $M_T = l_{\max} + 1$ along the delay axis and $N_T = 2k_{\max} + 1$ along the Doppler axis. The corresponding index sets for channel estimation are defined as

$$\mathcal{E}_m = \left[m_p, (m_p + l_{\max})_M\right],\ \mathcal{E}_n = \left[(n_p - k_{\max})_N, (n_p + k_{\max})_N\right].$$

Accordingly, the received signal in the estimation region based on Eqs. (11) and (15) is given by

$$\mathbf{Y}_{\mathrm{dd}}[m,n] = \frac{1}{N} x_p h_{\mathrm{LoS},m_p}\, \zeta_N(k_{\mathrm{LoS},n_p} - n)\ \mathrm{sinc}\left(m - l_{\mathrm{LoS},m_p}\right),\ (m,n) \in \mathcal{E}_m \times \mathcal{E}_n \tag{16}$$

where the effective channel gain is defined as $h_{\mathrm{LoS},m_p} = h_{\mathrm{LoS}}\, e^{j2\pi \frac{k_{\mathrm{LoS}} m_p}{MN}}$, $k_{\mathrm{LoS},n_p} = k_{\mathrm{LoS}} + n_p$ and $l_{\mathrm{LoS},m_p} = l_{\mathrm{LoS}} + m_p$. In (16), we omit the contribution of noise and interference from data symbols within the estimation region. This assumption is consistent with the modeling approach adopted throughout the paper and allows us to focus on the dominant channel effects relevant to pilot-based estimation. Equation (16) shows that the observed channel impulse response at the receiver exhibits a periodic sinc behavior along the Doppler dimension and a sinc behavior along the delay dimension. Later, we show that frequency estimation for a complex sinusoidal signal can be interpreted as estimating the true frequency from samples of the periodic sinc function $\zeta(\cdot)$, an approximation that is also aligned with related modeling approaches in the literature, where periodic sinc functions are used along both the delay and Doppler dimensions[13–16].

We now approximate the $\mathrm{sinc}(x)$ function using the periodic function $\zeta_M(x)$. Using the first-order Taylor expansion $\sin(\pi x/M) \approx \pi x/M$, we obtain

$$\mathrm{sinc}(x) \simeq \frac{\sin(\pi x)}{M \sin(\pi x/M)} = \frac{\zeta_M(x)}{M}\, e^{-j\pi x(M-1)/M}, \tag{17}$$

which holds for $|x| \ll M$. Then, the received signal based on (16) and (17) becomes

$$\begin{aligned} \mathbf{Y}_{\mathrm{dd}}[m,n] \simeq\ & \tfrac{1}{MN} x_p h_{\mathrm{LoS},m_p} e^{\frac{-j\pi l_{\mathrm{LoS},m_p}(M-1)}{M}} \zeta_N(k_{\mathrm{LoS},n_p} - n) \\ & \zeta_M(l_{\mathrm{LoS},m_p} - m)\, e^{\frac{j\pi m(M-1)}{M}},\ (m,n) \in \mathcal{E}_m \times \mathcal{E}_n \end{aligned} \tag{18}$$

In Fig. 4, we illustrate the effect of fractional delay, specifically for a delay value of 3.2, while the Doppler shift is assumed to be an integer. A similar behavior applies to fractional Doppler if we take a cross-section along the Doppler axis at a fixed delay. The sampling points at integer values capture the so-called virtual taps. In ref. 8, the virtual taps are treated as actual

channel taps. However, as we have discussed, these virtual taps fail to accurately represent the true delay and Doppler characteristics of the channel, which introduces limitations in data detection. We will demonstrate this claim through simulation results presented in the Results section. The figure highlights how closely $\zeta(x)$ approximates the sinc function. As seen near the peak, the sinc and $\zeta(x)$ functions closely match, which is important since most of the signal power is concentrated there. Although they diverge slightly away from the peak, this has minimal impact due to the low power in those regions. Now that the input-output relation in the DD domain (i.e., the channel impulse response in the DD domain) exhibits the form of a periodic sinc function $\zeta(\cdot)$ along both delay and Doppler, the channel estimation problem can be naturally interpreted as a frequency estimation task.

Building on this interpretation, we next provide a detailed description of the A&M frequency estimation algorithm. In ref. 21, the authors introduced the A&M algorithm for estimating the frequency f of a complex sinusoidal signal defined as

$$\mathbf{s}[n] = Ae^{j2\pi\frac{f}{F_s}n} + \mathbf{w}[n]; n = 0, \ldots, N-1, \tag{19}$$

where $\mathbf{w}[n]$ denotes zero-mean additive white Gaussian noise and F_s is the sampling frequency. The frequency f is decomposed into integer and fractional components as follows

$$f = \frac{f_I + f_F}{N} F_s, \tag{20}$$

with $f_I \in \mathbb{Z}$ and $f_F \in [-0.5, 0.5]$ representing the integer and fractional parts, respectively.

To estimate the frequency f, the A&M method processes the DFT samples of the signal $\mathbf{s}[n]$. The DFT of the signal $\mathbf{s}[n]$ yields its frequency-domain representation as

$$\mathbf{s}'[k] = A\,\zeta_M(f-k). \tag{21}$$

which corresponds to a sampled version of the periodic sinc function, similar to the behavior observed in the DD channel impulse response.text

Subsequently, Solak et al.[25] proposed the HAQSE method for estimating 2D sinusoidal components. Building upon these foundations, we propose a 2D extension of the A&M algorithm for estimating DD channel parameters.

By comparing (18) and (21), it can be observed that the received signal $\mathbf{Y}_{dd}[m, n]$ along the Doppler dimension exhibits the same structure as the DFT representation of a sinusoidal signal $\mathbf{s}'[k]$. Along the delay dimension, the structure remains similar, except for a phase shift given by $e^{\frac{j\pi m(M-1)}{M}}$. The term $\frac{1}{N}x_p h_{\mathrm{LoS},m_p} e^{\frac{-j\pi l_{\mathrm{LoS},m_p}(M-1)}{M}}$ is a constant with respect to both m and n, and therefore does not affect the signal's variation along these dimensions.

In the following, we propose a 2D A&M-based method for channel parameter estimation, inspired by the 2D frequency estimation approach presented in ref. 25. Unlike that work, instead of processing the entire 2D matrix, we focus only on the row and column corresponding to the highest value, which significantly reduces computational complexity.

To focus on the estimation area within the received DD domain matrix $\mathbf{Y}_{\mathrm{dd}}$, we construct a new matrix $\mathbf{Y}_{\mathrm{ext}} \in \mathbb{C}^{M\times N}$. This matrix extracts and retains only the elements of $\mathbf{Y}_{\mathrm{dd}}$ located at indices $(m, n) \in \mathcal{E}_m \times \mathcal{E}_n$. All other entries are set to zero. We define

$$\mathbf{Y}_{\mathrm{ext}}(m,n) = \begin{cases} \mathbf{Y}_{\mathrm{dd}}(m,n), & (m,n) \in \mathcal{E}_m \times \mathcal{E}_n \\ 0, & \text{otherwise} \end{cases} \tag{22}$$

To estimate the Doppler shift, we first identify the delay and Doppler indices corresponding to the peak magnitude of the received signal, defined as

$$\widehat{l}_{\mathrm{LoS},m_p,I}, \widehat{k}_{\mathrm{LoS},n_p,I} = \underset{m,n}{\mathrm{argmax}} \left|\mathbf{Y}_{\mathrm{ext}}(m,n)\right| \tag{23}$$

These indices serve as estimates of the integer components of the delay l_{LoS,m_p} and Doppler shifts k_{LoS,n_p}. The reliability of this peak detection is valid only when the received SNR is above the ML threshold[21,24].

Next, we compute the N-point IDFT of the sequence $\mathbf{Y}_{\mathrm{ext}}[\widehat{l}_{\mathrm{LoS},m_p,I}, :]$, given by

$$\mathbf{y}_{t,\mathrm{Doppler}} = \mathbf{F}_N^H \mathbf{Y}_{\mathrm{dd}}[\widehat{l}_{\mathrm{LoS},m_p,I}, :]^T \in \mathbb{C}^{N\times 1} \tag{24}$$

Here, the subscript t in $\mathbf{y}_{t,\mathrm{Doppler}}$ denotes that this signal represents the equivalent time-domain form of the frequency-domain vector $\mathbf{Y}_{\mathrm{dd}}[\widehat{l}_{\mathrm{LoS},m_p,I}, :]^T$. Note that in (24) we only use one row of $\mathbf{Y}_{\mathrm{dd}}$. The reason for this dimensionality reduction is that, as seen in (16), the received signal along delay and Doppler are independent. Each row and each column contains all the information about the Doppler and delay of the channel taps, respectively. Therefore, the estimation of delay and Doppler can be performed independently, with reduced processing dimension.

The algorithm proceeds iteratively. At each iteration, the goal is to estimate the fractional Doppler component, denoted by $k_{\mathrm{LoS},n_p,F}$. To this end, during the ith iteration, we compute the DTFT of the time-domain vector $\mathbf{y}_{t,\mathrm{Doppler}}$ within an α-neighborhood centered around the current estimate $\widehat{k}_{\mathrm{LoS},n_p,I} + \widehat{k}^{i-1}_{\mathrm{LoS},F}$.

$$y^i_{\pm\alpha,\,\mathrm{Doppler}} = \frac{1}{\sqrt{N}} \sum_{n=0}^{N-1} \mathbf{y}_{t,\mathrm{Doppler}}[n] e^{-j2\pi\frac{\widehat{k}_{\mathrm{LoS},n_p,I} + \widehat{k}^{i-1}_{\mathrm{LoS},F} \pm \alpha}{N} n} \tag{25}$$

where the value of $\alpha = 0.5$, and $\widehat{k}^{i-1}_{\mathrm{LoS},F}$ denotes the fractional Doppler estimated in the previous iteration[21]. The choice of $\alpha = 0.5$ follows the canonical half-bin offset used in the original A&M estimator for fractional frequency estimation[21]. This value allows a closed-form recovery of the fractional component in the noise-free case, as it symmetrically samples the DTFT around the dominant DFT bin. While other estimators may use different offsets, $\alpha = 0.5$ is standard within the A&M framework and ensures accurate fractional delay and Doppler estimation. The impact of different α values is discussed in ref. 25. The updated estimate of the fractional Doppler component at iteration i, denoted by $\widehat{k}^i_{\mathrm{LoS},F}$, is computed as

$$\widehat{k}^i_{\mathrm{LoS},F} = \alpha\,\Re\left\{\frac{y^i_{+\alpha,\,\mathrm{Doppler}} + y^i_{-\alpha,\mathrm{Doppler}}}{y^i_{+\alpha,\mathrm{Doppler}} - y^i_{-\alpha,\mathrm{Doppler}}}\right\} + \widehat{k}^{i-1}_{\mathrm{LoS},F}, \tag{26}$$

Finally, the estimated Doppler value after subtracting the pilot location along Doppler is given by

$$\widehat{k}_{\mathrm{LoS}} = \widehat{k}_{\mathrm{LoS},n_p,I} + \widehat{k}^{i_{\mathrm{A\&M}}}_{\mathrm{LoS},F} - n_p, \tag{27}$$

where $i_{\mathrm{A\&M}}$ denotes the final iteration index of A&M algorithm. Equation (26) provides a closed-form solution, derived in ref. 21, for estimating the true frequency value using the DTFT of the signal evaluated at the 0.5-offset neighboring points of the integer part of the desired frequency. The formulation is then extended to an arbitrary offset value α[22].

The estimation procedure for fractional delay closely resembles that of fractional Doppler estimation, with the exception that an additional phase shift term, $e^{\frac{j\pi m(M-1)}{M}}$, discussed in System Model, must be

incorporated. To perform the estimation, we extract the received signal along the delay axis corresponding to the index of the maximum integer Doppler, denoted by $\widehat{k}_{\mathrm{LoS},n_p,I}$. The phase compensation is then applied as follows

$$\mathbf{y}_{l,\mathrm{pc}} = \mathbf{P}\mathbf{Y}_{\mathrm{ext}}[:,\widehat{k}_{\mathrm{LoS},n_p,I}] \in \mathbb{C}^{M\times 1} \tag{28}$$

where $\mathbf{P} = \mathrm{diag}\,(e^{j\pi m\frac{M-1}{M}})$ for $m = 0, \ldots, M-1$. Here, the subscripts l and "pc" indicate that the signal is taken along the delay axis and has been phase-compensated, respectively. To estimate the fractional delay, we apply the same algorithm used for Doppler estimation. Specifically, we compute the IDFT of $\mathbf{y}_{l,\mathrm{pc}}$ as follows

$$\mathbf{y}_{t,\mathrm{delay}} = \mathbf{F}_M^H \mathbf{y}_{l,\mathrm{pc}} \in \mathbb{C}^{M\times 1} \tag{29}$$

Next, we evaluate the DTFT of $\mathbf{y}_{t,\mathrm{delay}}$ within an α-neighborhood centered around $\widehat{l}_{\mathrm{LoS},m_p,I} + \widehat{l}^{\,i-1}_{\mathrm{LoS},F}$, where $\widehat{l}^{\,i-1}_{\mathrm{LoS},F}$ denotes the fractional delay estimated in the $(i-1)$th iteration.

$$y^{i}_{\pm\alpha,\,\mathrm{delay}} = \frac{1}{\sqrt{M}}\sum_{m=0}^{M-1}\mathbf{y}_{t,\mathrm{delay}}[m]\, e^{-j2\pi\frac{\widehat{l}_{\mathrm{LoS},m_p,I}+\widehat{l}^{\,i-1}_{\mathrm{LoS},F}\pm\alpha}{M}m}. \tag{30}$$

To estimate the fractional delay component at the current iteration, we use the following expression

$$\widehat{l}^{\,i}_{\mathrm{LoS},F} = \alpha\,\Re\left\{\frac{y_{+\alpha,\mathrm{delay}} + y_{-\alpha,\mathrm{delay}}}{y_{+\alpha,\mathrm{delay}} - y_{-\alpha,\mathrm{delay}}}\right\} + \widehat{l}^{\,i-1}_{\mathrm{LoS},F} \tag{31}$$

After estimating the fractional delay, the total delay is obtained by adjusting the location of the pilot as

$$\widehat{l}_{\mathrm{LoS}} = \widehat{l}_{\mathrm{LoS},m_p,I} + \widehat{l}^{\,i_{\mathrm{A\&M}}}_{\mathrm{LoS},F} - m_p \tag{32}$$

The parameters required for complete channel estimation are the delay, Doppler, and channel gain. To estimate the gain, we first compensate for the additional phase shift introduced in (18). This is done by applying a 2D IDFT to the phase-compensated received signal in the DD domain. The resulting matrix is then projected onto the estimated delay and Doppler values. Specifically, the phase shift $e^{-j2\pi m\frac{M-1}{M}}$, discussed in Channel Estimation - LOS Scenario, corrects the distortion described in (18), leading to

$$\mathbf{Y}_{\mathrm{pc}} = \mathbf{F}_M^H\,\mathbf{P}\,\mathbf{Y}_{\mathrm{ext}}\,\mathbf{F}_N^H \in \mathbb{C}^{M\times N}, \tag{33}$$

where the subscript "pc" denotes the phase-compensated received matrix.

Next, we project the signal onto the estimated subspace[24]

$$\widehat{h}_{\mathrm{LoS},m_p} = \frac{1}{MN}\sum_{n=0}^{N-1}\sum_{m=0}^{M-1}\mathbf{Y}_{\mathrm{pc}}[m,n]\, e^{-j2\pi\frac{\widehat{l}_{\mathrm{LoS},m_p}}{M}m}\, e^{-j2\pi\frac{\widehat{k}_{\mathrm{LoS},n_p}}{N}n}, \tag{34}$$

and the gain h_{LoS} is estimated by applying a phase compensation to $\widehat{h}_{\mathrm{LoS},m_p}$ as

$$\widehat{h}_{\mathrm{LoS}} = \widehat{h}_{\mathrm{LoS},m_p}\, e^{-j2\pi\frac{\widehat{k}_{\mathrm{LoS},m_p}}{MN}}. \tag{35}$$

Since the pilot location is set to $m_p = 0$, the dependency of the channel gain estimation in (35) is reduced. You can find in Algorithm 1, the proposed parameter estimation for DD channel for LoS case.

Algorithm 1. Calculate channel parameters in LoS scenario

Require: $\mathbf{Y}_{\mathrm{ext}}$; $i_{\mathrm{A\&M}}$; $\hat{k}^0_{\mathrm{LoS},F} = 0$; $\hat{l}^0_{\mathrm{LoS},F} = 0$.
Ensure: $\widehat{l}_{LoS}, \widehat{k}_{LoS}, \widehat{h}_{LoS}$.
1: $\widehat{l}_{\mathrm{LoS},m_p,I}, \widehat{k}_{\mathrm{LoS},n_p,I} \Leftarrow$ Equation (23)
2: $\mathbf{y}_{t,\mathrm{Doppler}} \Leftarrow$ Equation (24)
3: $\mathbf{y}_{l,\mathrm{pc}} \Leftarrow$ Equation (28)
4: $\mathbf{y}_{t,delay} \Leftarrow$ Equation (29)
5: **for** $i = 1, \ldots, i_{\mathrm{A\&M}}$ **do**
6: $\quad y^{i}_{\pm\alpha,\,\mathrm{Doppler}} \Leftarrow$ Equation (25)
7: $\quad \widehat{k}^{i}_{\mathrm{LoS},F} \Leftarrow$ Equation (26)
8: $\quad y^{i}_{\pm\alpha,\,\mathrm{delay}} \Leftarrow$ Equation (30)
9: $\quad \widehat{l}^{\,i}_{\mathrm{LoS},F} \Leftarrow$ Equation (31)
10: **end for**
11: $\widehat{k}_{\mathrm{LoS}} \Leftarrow$ Equation (27)
12: $\widehat{l}_{\mathrm{LoS}} \Leftarrow$ Equation (32)
13: $\mathbf{Y}_{\mathrm{pc}}[m,n] \Leftarrow$ Equation (33)
14: $\widehat{h}_{\mathrm{LoS},m_p} \Leftarrow$ Equation (34)
15: $\widehat{h}_{\mathrm{LoS}} \Leftarrow$ Equation (35)

Channel estimation - NLOS scenario

In this subsection, we present the received signal model in the DD domain in the presence of multiple channel taps. We then introduce the iterative 2D A&M algorithm used to estimate the channel parameters.

In the presence of an NLoS channel, the received signal resulting from the transmission of the pilot defined in (15) is given by

$$\mathbf{Y}_{\mathrm{dd}}[m,n] = \frac{1}{MN}x_p\sum_{i=1}^{P}h_{i,m_p}e^{\frac{-jnl_{i,m_p}(M-1)}{M}}\zeta_N(k_{i,n_p}-n)\,\zeta_M(l_{i,m_p}-m)\,e^{\frac{j\pi m(M-1)}{M}} \tag{36}$$

where $l_{i,m_p} = l_i + m_p$ and $k_{i,n_p} = k_i + n_p$. The NLoS scenario is illustrated in Fig. 2, where the receiver inside a car obtains positioning information through a multipath channel.

To estimate the channel parameters in an NLoS scenario, we adopt an iterative approach. In each iteration, Algorithm 1 is applied to estimate the parameters of the strongest path. The path with the highest gain is identified, its contribution is subtracted from the received signal, and the process continues with the next strongest path. The total number of iterations is P, corresponding to the number of significant paths. The signal update at iteration i is given by

$$\mathbf{Y}^{i}[m,n] = \mathbf{Y}^{i-1}_{\mathrm{ext}}[m,n] - \frac{1}{MN}x_p\widehat{h}_{i,m_p}e^{\frac{-jn\widehat{l}_{i,m_p}(M-1)}{M}}\zeta_N(\widehat{k}_{i,n_p}-n)\,\zeta_M(\widehat{l}_{i,m_p}-m)\,e^{\frac{j\pi m(M-1)}{M}} \tag{37}$$

for $m = 0, \ldots, M-1$ and $n = 0, \ldots, N-1$, where $\mathbf{Y}^{i-1}_{\mathrm{ext}}[m,n]$ is the retained signal extracted from $\mathbf{Y}^{i}[m,n]$, as defined in Eq. (22), and the initial condition is $\mathbf{Y}^{0}[m,n] = \mathbf{Y}_{\mathrm{dd}}[m,n]$. This process is repeated P times until all channel parameters are estimated.

Following ref. 24, we assume the number of channel taps is known, which simplifies the estimation process. When this information is unavailable, the method proposed in refs. 27–31 can be used to estimate the number of taps effectively. In practical scenarios where the number of taps is not specified, established model order selection techniques such as the generalized Akaike information criterion (GAIC) or minimum description length (MDL) can be applied as a preprocessing step to estimate the number of taps, as discussed in refs. 27,28. To assess the robustness of our A&M method under unknown tap conditions, we include a simulation where the number of taps is estimated using a simple formula defined in the context of compressed sensing, following refs. 14–16. The results show that A&M remains effective even without prior knowledge of the tap count.

Table 1 | Comparison of computational complexity between the proposed A&M method and state-of-the-art channel estimation techniques

Algorithm	Number of complex multiplications
Embedded[8]	$M_T N_T$
Proposed A&M LOS	$MN(1+\frac{1}{2}\log_2 M+\frac{1}{2}\log_2 N)+M(2+\frac{1}{2}\log_2 M)+N(1+\frac{1}{2}\log_2 N)$
Proposed A&M NLOS	$\widehat{P}\big(MN(1+\frac{1}{2}\log_2 M+\frac{1}{2}\log_2 N)+M(2+\frac{1}{2}\log_2 M)+N(1+\frac{1}{2}\log_2 N)\big)$
OGSBI[14]	$\frac{2}{3}(M_T N_T)^3+2M_\tau N_\nu(M_T N_T)^2+\big(2(M_\tau N_\nu)^2+4M_\tau N_\nu+1\big)M_T N_T$
	$+(M_\tau N_\nu)^2+4M_\tau N_\nu+2\widehat{P}(\widehat{P}+1)$
GESBI[15]	$N_{\text{exter}}\big(2M_T N_T M_\tau N_\nu+N_{\text{inter1}}\big(\frac{2}{3}(M_T N_T)^3+2M_\tau N_\nu(M_T N_T)^2$
	$+\big(2(M_\tau N_\nu)^2+4M_\tau N_\nu+1\big)M_T N_T+(M_\tau N_\nu)^2+4M_\tau N_\nu$
	$+2\widehat{P}(\widehat{P}+1)\big)\big)$
T-GEESBI[16]	$N_{\text{exter}}\big(2M_T N_T M_\tau N_\nu+N_{\text{inter1}}\big((3+M_T N_T)(M_\tau N_\nu)^2$
	$+M_\tau N_\nu(12+M_T N_T)+2M_T N_T+2\widehat{P}(\widehat{P}+1)\big)\big)$
GRASBI[13]	$N_{\text{exter}}\Big(2\widehat{P}N_{\text{inter2}}\Big(3(M_T N_T)^2+2M_T N_T+\widehat{M}\widehat{N}\Big)\cdot$
	$+N_{\text{inter1}}\big(\frac{2}{3}(M_T N_T)^3+2(M_T N_T)^2 M_\tau N_\nu+(M_\tau N_\nu)^2 M_T N_T$
	$+4M_T N_T M_\tau N_\nu+4M_\tau N_\nu+M_T N_T\big)\big)$
T-GRAESBI[13]	$N_{\text{exter}}\Big(2\widehat{P}N_{\text{inter2}}\Big(3(M_T N_T)^2+2M_T N_T+\widehat{M}\widehat{N}\Big)$
	$+N_{\text{inter1}}\big((3+M_T N_T)(M_\tau N_\nu)^2+M_\tau N_\nu(12+M_T N_T)$
	$+2M_T N_T+2\widehat{P}(\widehat{P}+1)\big)\big)$

Table 2 | Parameter settings used to calculate number of complex multiplications.

Param.	M	N	$\widehat{P}$	M_T	N_T	M_τ	N_ν	N_{inter1}	N_{inter2}	N_{exter}
Value	64	16	5	4	5	10	10	500	10	10

Algorithm 2. Calculate channel parameters in NLoS scenario
Require: $\mathbf{Y}^0[m,n]$; $i_{\text{A\&M}}$; $\hat{l}_{i,F}^0=0$, $\hat{k}_{i,F}^0=0$, for $i=1,\ldots,P$.
Ensure: $\widehat{l}_i$, $\widehat{k}_i$, $\widehat{h}_i$; for $i=1,\ldots,P$.
1: **for** $i=1,\ldots,P$ **do**
2: $\widehat{k}_i,\widehat{l}_i,\widehat{h}_i \Leftarrow$ Apply Algorithm 1 on $\mathbf{Y}^{i-1}[m,n]$
3: $Y_i[m,n] \Leftarrow$ Equation (37)
4: **end for**

You can find in Algorithm 2, the proposed parameter estimation algorithm for DD channel for NLoS case.

Computational complexity

The computational complexity of estimating the channel parameters in the LoS case from the received matrix $\mathbf{Y}_{\text{dd}}$ can be divided into three stages: Doppler estimation, delay estimation, and gain estimation.

Doppler estimation involves computing a fast Fourier transform (IFFT), which requires approximately $\frac{N}{2}\log_2 N$ complex multiplications, as shown in (24), and evaluating a DTFT at a specific point in (25), which adds N complex multiplications. Delay estimation includes an additional M complex multiplications for phase compensation, as described in (28). For gain estimation, phase compensation involves a matrix multiplication with a diagonal matrix $\mathbf{P}$, requiring MN complex multiplications. This is followed by a 2D IFFT„ which requires approximately $\frac{MN}{2}(\log_2 M+\log_2 N)$ complex multiplications, as shown in (33), and a 2D projection step with another MN complex multiplications. Thus, the total number of complex multiplications for gain estimation is $MN(1+\frac{1}{2}\log_2 M+\frac{1}{2}\log_2 N)+M(2+\frac{1}{2}\log_2 M)+N(1+\frac{1}{2}\log_2 N)$ In the NLoS case, the procedure is similar but repeated over P iterations.

Table 3 | Number of complex multiplication for each algorithm based on defined parameter in Table 2

Algorithm	Number of complex multiplications
Proposed A&M LOS	6.512×10^3
Proposed A&M NLOS	3.256×10^4
OGSBI[14]	5.038×10^5
GESBI[15]	2.519×10^9
T-GEESBI[16]	1.167×10^9
GRASBI[13]	1.581×10^9
T-GRAESBI[13]	1.279×10^9

Table 1 compares the computational complexity of our proposed A&M estimator, off-grid SBL-based methods, and EP estimation. Parameters M_τ and N_ν represent the super-resolution grid sizes[13]. The iteration counts N_{inter1}, N_{inter2}, and N_{exter} correspond to internal SBL operations, grid refinement [13], and external loops, respectively. As a concrete example, we computed the number of multiplications for the same scenario shown in Fig. 6a (in Results section), where normalized mean square error (NMSE) performance is illustrated. The parameters used in this simulation scenario are listed in Table 2, and based on these parameters, the number of complex multiplications required for each algorithm is shown in Table 3. Our A&M method outperforms other off-grid approaches with lower complexity, slightly higher than EP, which suffers from poor detection due to its inability to estimate true delay and Doppler values.

Results

To validate the proposed channel estimation method, we first performed simulations in MATLAB to demonstrate its effectiveness and to confirm its applicability to realistic scenarios. These simulations served as a foundation for transitioning to a practical setup. To further validate the approach, an SDR-based setup was implemented, as shown in Fig. 5. It consists of an Ettus USRP B210 SDR connected to a PC via USB 3.0 for sample transmission and

reception. A MATLAB-generated OTFS signal, similar to the simulation setup, is sent through a Simulink-controlled transmission chain, enabling real-world testing of the proposed algorithm.

MATLAB implementation

The performance of the proposed methods is evaluated through MATLAB-based simulations. The carrier frequency is set to 4 GHz, and the EVA channel model is adopted to reflect realistic multipath conditions[32]. Simulations are conducted across multiple frame configurations with varying values of (M, N). The sub-carrier space is assumed to be $\Delta f = 15$ kHz. The power of the pilot symbol is chosen such that $10\log_{10}\left(\frac{|x_p|^2}{\mathbb{E}[|x_d|^2]}\right) = 30$ dB, where $|x_p|^2$ is the pilot power and $\mathbb{E}[|x_d|^2]$ is the average power of the data symbols. The SNR is defined as $\text{SNR} = \frac{\mathbb{E}[|x_d|^2]}{\sigma_n^2}$, where σ_n^2 is the variance of the additive white Gaussian noise (AWGN). The maximum velocity in the environment is set to 500 km/h. Detection is performed using minimum mean square error (MMSE) matrix equalization. The simulation results include both NMSE and BER, depending on the evaluation scenario. The NMSE of the channel is defined as $\text{NMSE} = \frac{\left\|\mathbf{h}_{m,n}[m\prime,n\prime]-\widehat{\mathbf{h}}_{m,n}[m\prime,n\prime]\right\|_F^2}{\left\|\mathbf{h}_{m,n}[m\prime,n\prime]\right\|_F^2}$, while the NMSE for delay and Doppler parameters is given by $\text{NMSE} = \frac{\left\|\mathbf{x}-\widehat{\mathbf{x}}\right\|_2^2}{\|\mathbf{x}\|_2^2}$, where $\mathbf{x}$ and $\widehat{\mathbf{x}}$ denote the true and estimated values, respectively. Unless otherwise specified, the same metric and simulation parameters apply across all figures. Our proposed method is labeled as **A&M**, assuming a periodic sinc structure ζ along the delay axis, while **A&M Sinc Approx.** refers to a variant where the channel follows a true sinc function, serving as an approximation to the A&M algorithm. These are compared against several existing approaches, including GESBI[15], OGSBI[14], T-GEESBI[16], GRASBI[13], T-GRAESBI[13], the conventional EP method[8], and Genie Bound I calculated in ref. 16.

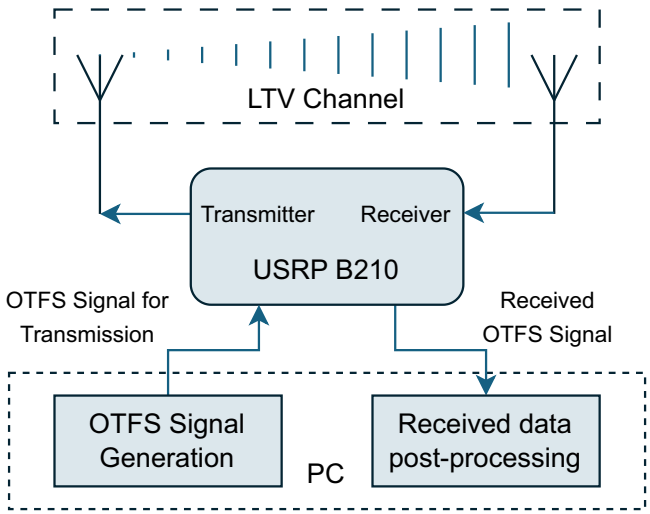


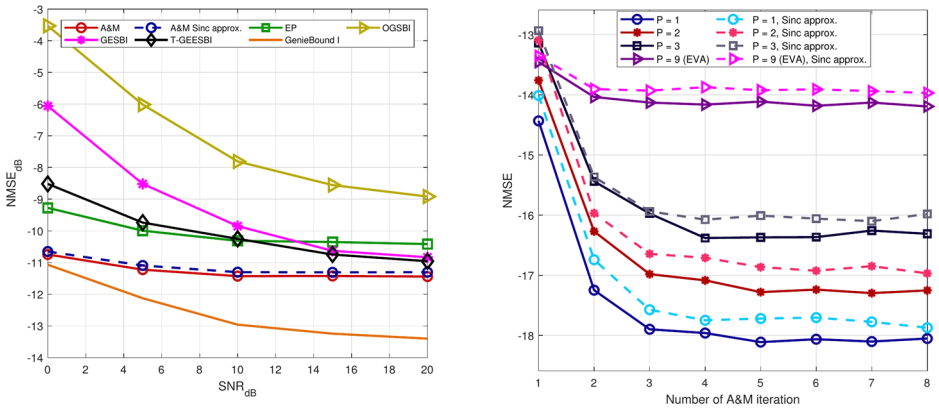
Fig. 5 | SDR-based implementation of the proposed OTFS system. A MATLAB-generated OTFS signal is transmitted and received using the USRP B210 connected to a PC via USB 3.0. The PC handles signal generation and post-processing, while the LTV channel represents the wireless propagation environment. This setup allows real-world testing of the proposed channel estimation and data detection algorithms. The figure was generated using Microsoft PowerPoint.

Figure 6a shows the NMSE curves for $\mathbf{h}_{m,n}[m\prime, n\prime]$ versus SNR with parameters defined in Table 2. The results correspond to an NLoS channel modeled by EVA. Our proposed A&M method achieves superior performance, consistently closer to the Genie Bound I defined in ref. 16, while have low-complexity to other well-known off-grid methods. Even when using an approximate model for A&M algorithm, as in the A&M Sinc Approx. variant which models the true channel behavior, the performance gap remains negligible. Although the EP scheme shows low estimation error due to its single-tap approach, it fails to capture the true delay and Doppler value. As discussed in System Model, this leads to phase misalignment in symbol detection, which will be reflected in the BER results presented later.

In Fig. 6b, the NMSE performance of the proposed A&M algorithm is shown as a function of the number of iterations at SNR = 20 dB. The evaluation assumes the number of channel taps is known at the receiver, allowing us to isolate and assess the impact of iteration count. Four-channel scenarios are considered: a LoS case (single tap) and NLoS cases with 2, 3, and 9 taps based on the EVA model. Each case includes both the original A&M and its Sinc approximation. It is evident that increasing the number of iterations beyond 2 offers limited improvement, especially for channels with more taps. This is because the maximum delay spread is the same for all cases, so increasing the number of taps makes them more closely spaced, which makes correct peak detection more difficult. Additionally, the performance gap between A&M and its Sinc approximation becomes negligible as the number of taps increases, likely due to the dominant interference from other taps overshadowing the side-lobe differences between the sinc and ζ functions. Comparing the EVA case at 2 iterations in Fig. 6b with the performance of our proposed method in Fig. 6a at SNR = 20 dB reveals that more accurate estimation of the number of taps could yield up to 1.5 dB improvement in NMSE.

Figure 7 compares the NMSE of delay and Doppler estimation. The parameters are the same as in Table 2, except for $(M, N) = (32, 32)$ and $N_{\text{exter}} = 5$. The simulation considers 4-channel taps uniformly distributed along both delay and Doppler axes, allowing a balanced evaluation of estimation performance. The results clearly demonstrate that our proposed method outperforms all other off-grid techniques in delay estimation.

Fig. 6 | NMSE performance evaluation of the estimated channel $\mathbf{h}_{m,n}[m\prime, n\prime]$ for $(M, N) = (60, 16)$. Subfigure **a** shows performance across SNR values for various estimation schemes, while **b** illustrates the impact of iteration count and approximation under different channel tap conditions. The figure was generated using MATLAB.



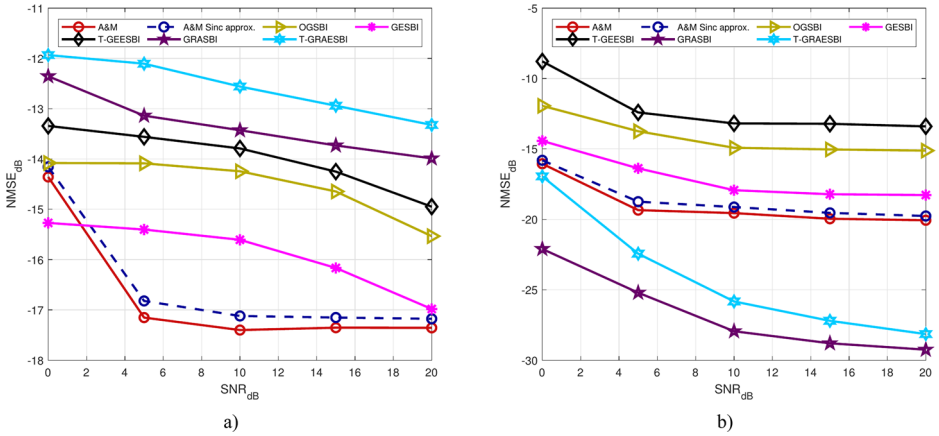


Fig. 7 | Comparison of $NMSE_{dB}$ performance versus SNR_{dB} using different off-grid methods. **a** NMSE of delay parameters estimation and **b** NMSE of Doppler parameters estimation. The figure was generated using MATLAB. Solid red circles: A&M method (sinc approximation exact); dashed dark blue circles: A&M method (approximate); solid yellow triangles: OGSBI; solid purple asterisks: GESBI; solid black diamonds: T-GEESBI; solid violet pentagrams: GRASBI; solid light blue hexagrams: T-GRAESBI.

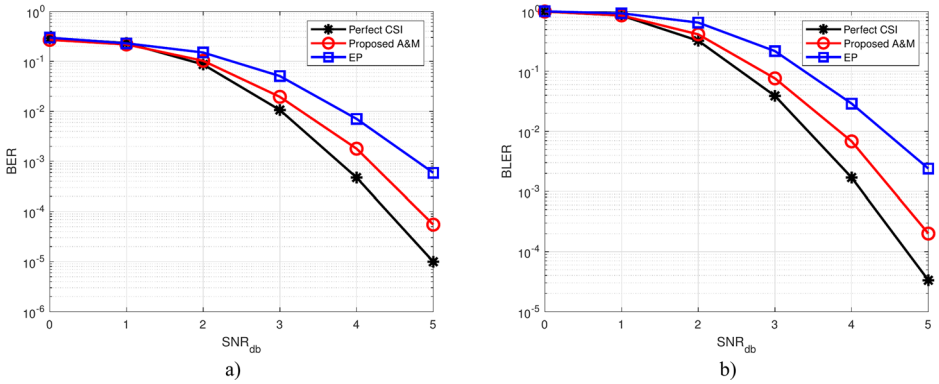


Fig. 8 | Performance comparison of the proposed A&M channel estimation method with EP and perfect CSI. **a** shows BER versus SNR and **b** shows the BLER for the coded bits. The figure was generated using MATLAB. Solid black asterisks: perfect CSI; solid red circles: A&M method; solid blue squares: EP method.

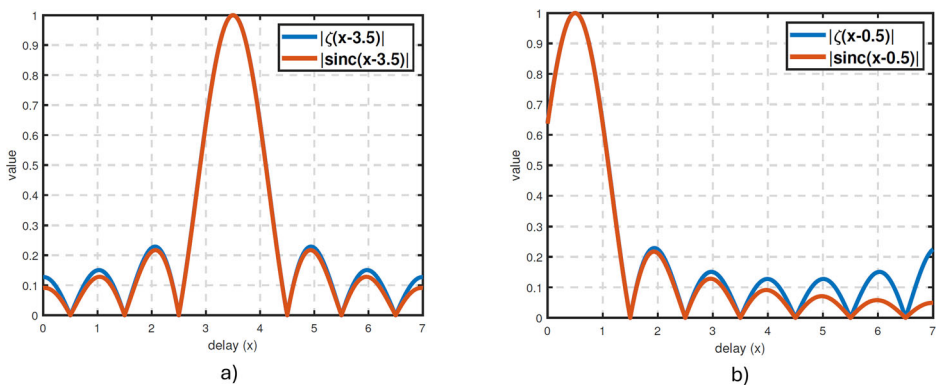


Fig. 9 | Comparison of the $\mathrm{sinc}(x - l_{\mathrm{LoS},m_p})$ and $\zeta(x - l_{\mathrm{LoS},m_p})$ functions for different LoS delays. **a** $l_{\mathrm{LoS},m_p} = 3.5$, corresponding to a small approximation error; and **b** $l_{\mathrm{LoS},m_p} = 0.5$, illustrating an edge mismatch. In both subfigures (**a**) and (**b**), the solid red line represents the $\mathrm{sinc}(x - l_{\mathrm{LoS},m_p})$ function, while the solid blue line represents the $\zeta(x - l_{\mathrm{LoS},m_p})$ function. The figures are generated using MATLAB.

While T-GRAESBI and GRASBI achieve strong Doppler estimation, their performance in delay estimation is significantly weaker. In contrast, our method delivers consistently high accuracy in both delay and Doppler domains, making it a more balanced and effective solution for joint delay and Doppler estimation tasks. The A&M Sinc Approx. variant almost matches the performance of A&M, confirming its robustness.

Figure 8 illustrates the BER and block error rate (BLER) performance of the proposed A&M method, benchmarked against both perfect CSI and the EP approach. The scenario is coded using LDPC with a code length of 10,560 and a rate of 1/3, as specified in TS 38.212 Section 5.3.2[33], with configuration parameters $(M, N) = (16, 16)$. Although the EP method achieves good channel-estimation accuracy, as shown in Fig. 6a, its BER and BLER performance consistently falls behind the proposed A&M method. This behavior reinforces the discussion provided in the Methods section: the embedded pilot-based estimator minimizes estimation error at the pilot locations, but the resulting channel estimate does not generalize well across data symbols that occupy different delay positions and therefore experience different phase rotations. Consequently, this mismatch degrades detection performance, even when the estimated channel appears accurate in a per-tap sense. This performance gap is evident and consistent in both BER and BLER curves, as shown in Fig. 8a, b, respectively.

We now analyze the validity of the approximation used in (17). From (16) and (18), the argument of both the sinc function and the periodic ζ-function is $m - l_{\mathrm{LoS},m_p}$. In the OTFS system, this quantity determines the degree to which the periodic approximation remains accurate. For a fixed M, the approximation is reliable when $\left|x - l_{\mathrm{LoS},m_p}\right| \ll M$. Therefore, the approximation error depends on the value of the received pilot location

l_{LoS,m_p} within one period $m \in [0, M-1]$. Figure 9 illustrates this behavior by plotting $\left|\mathrm{sinc}(m - l_{\mathrm{LoS},m_p})\right|$ and $\left|\zeta_M(m - l_{\mathrm{LoS},m_p})\right|$ for visual comparison. As shown in Fig. 9a, when l_{LoS,m_p} is near $M/2$, the approximation error at the edges of the interval is small. In contrast, Fig. 9b shows that when l_{LoS,m_p} lies close to the boundaries (0 or M), the approximation error increases significantly at the opposite edge.

To quantify the approximation error, Fig. 10 also plots the NMSE

$$\mathrm{NMSE}(l_{\mathrm{LoS},m_p}/M) = \int_0^M \frac{\left|\frac{\sin\left(\pi(x-l_{\mathrm{LoS},m_p})\right)}{M\sin\left(\frac{\pi(x-l_{\mathrm{LoS},m_p})}{M}\right)} - \mathrm{sinc}(x - l_{\mathrm{LoS},m_p})\right|^2}{\left|\frac{\sin\left(\pi(x-l_{\mathrm{LoS},m_p})\right)}{M\sin\left(\frac{\pi(x-l_{\mathrm{LoS},m_p})}{M}\right)}\right|^2} dx, \tag{38}$$

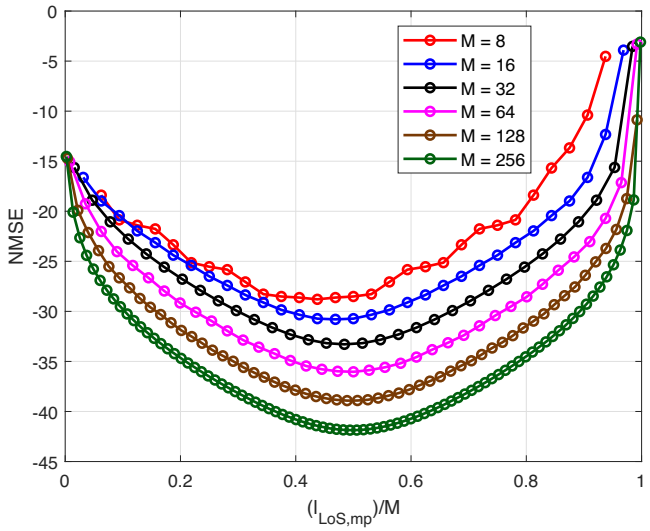


Fig. 10 | NMSE between the periodic sinc $\frac{\sin(\pi(m-l_{\mathrm{LoS},m_p}))}{M\sin(\pi(m-l_{\mathrm{LoS},m_p})/M)}$ and $\mathrm{sinc}(m - l_{\mathrm{LoS},m_p})$ versus $l_{\mathrm{LoS},m_p}/M$ for different values of M. The figure is generated using MATLAB. Solid red line: $M = 8$; solid blue line: $M = 16$; solid black line: $M = 32$; solid purple line: $M = 64$; solid brown line: $M = 128$; solid green line: $M = 256$. The figure was generated using MATLAB.

as a function of the delay-bin-normalized delay $l_{\mathrm{LoS},m_p}/M$ (DBN delay). The DBN delay is used instead of the normalized delay so that different values of M may be compared consistently.

Numerical results in Fig. 10 show that increasing M reduces the overall approximation error. For small M, the minimum approximation error is approximately -28 dB, and achieving an error below -20 dB requires $l_{\mathrm{LoS},m_p} \in [0.1M,\ 0.8M]$. For $M = 64$, the minimum error improves to about -36 dB, and the region where the error remains below -20 dB expands to $l_{\mathrm{LoS},m_p} \in [0.04M,\ 0.9M]$. For $M = 256$, the approximation becomes uniformly accurate: the error is below -20 dB for almost all values of l_{LoS,m_p}, with a minimum around -42 dB.

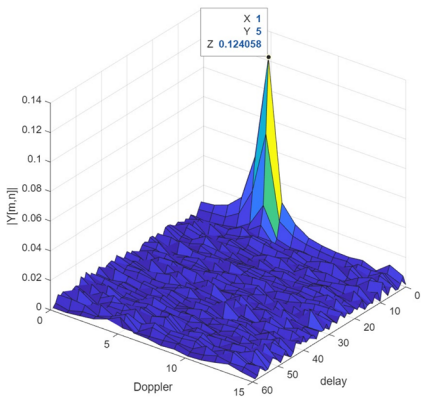
SDR-based implementation

Building on the simulation results, we implemented a real-world validation using an SDR-based setup. The carrier frequency is set to 2.4 GHz, with $\Delta f =$ 7.812 kHz and $(M, N) = (16, 16)$. The pilot symbol was placed at $(m_p, n_p) = (1, 8)$. A frequency deviation v_{sdr} between the transmitter and receiver carrier frequencies was introduced to emulate user equipment motion over a linear time-varying (LTV) channel. Frequency deviation is generated by keeping the transmitter's carrier frequency $f_{\mathrm{TX}} = f_c$ constant, while the receiver's carrier frequency is set to $f_{\mathrm{RX}} = f_c + v_{\mathrm{sdr}}$. These frequency values, defined in the software, are then sent to the device, which controls internal voltage-controlled oscillators (VCOs) to mix signals from baseband to passband at the transmitter and back to baseband at the receiver. The channel model corresponds to a line-of-sight (LoS) scenario using two identical omnidirectional 2.4 GHz antennas positioned 5 cm apart, resulting in negligible delay spread in the DD domain. Since the SDR experiment was not performed inside an anechoic chamber, nearby devices operating in the 2.4 GHz band introduced additional interference to the received signal. After transmission, the received OTFS signal is stored and processed using the proposed estimation algorithm followed by MMSE equalization, yielding the signal in the DD domain and the resulting 4-QAM constellation, shown in Fig. 11a, b. In this setup, the error vector magnitude (EVM) of the received symbols, over 1450 OTFS frames, was calculated in post-processing as 0.42 at an SNR of 12 dB, with a peak EVM of 1.87. The channel model is based on a LoS scenario.

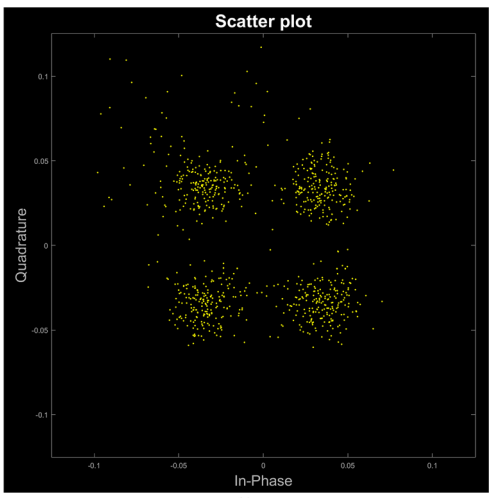
Discussion

In this paper, we proposed a fractional delay and Doppler channel estimation method based on A&M and the 2D HAQSE algorithm. Unlike methods that estimate virtual taps, our approach directly estimates the true delay, Doppler, and channel gain with high accuracy. To handle fractional delay, we employed a sinc-based approximation to the $\zeta(x)$ function and applied a phase compensation step to enable the use of the A&M algorithm.

Fig. 11 | Real-world validation of the proposed channel estimation. a Received signal in the DD domain, and **b** 4-QAM constellation after equalization. The figure was generated using MATLAB.



a)



b)

The proposed method maintains low complexity, in contrast to typical SBL-based off-grid estimation techniques, and achieves better performance than both EP and SBL-based methods. Good performance is obtained with only two iterations, making it suitable for practical deployment. We have validated our results through both MATLAB simulation and real-world implementation. An SDR setup was built using an Ettus USRP B210.

Data availability

There is no dataset generated or used in this work.

Code availability

The code used in this study is not publicly available.

Received: 15 August 2025; Accepted: 8 April 2026;
Published online: 04 August 2026

References

1. Zegrar, S. E., Sümer, A. S. & Arslan, H. Fractional delay and fractional Doppler estimation and mitigation framework in OTFS systems. *IEEE Trans. Veh. Technol.* **74**, 2884–2896 (2025).
2. Aldababsa, M., Özyurt, S., Kurt, G. K. & Kucur, O. A survey on orthogonal time frequency space modulation. *IEEE Open J. Commun. Soc.* **5**, 4483–4518 (2024).
3. Alwis, C. D. et al. Survey on 6g frontiers: trends, applications, requirements, technologies and future research. *IEEE Open J. Commun. Soc.* **2**, 836–886 (2021).
4. Hadani, R. et al. Orthogonal time frequency space modulation. In: *2017 IEEE Wireless Communications and Networking Conference (WCNC)*, pp. 1–6 (IEEE, 2017).
5. Wei, Z. et al. Orthogonal time-frequency space modulation: a promising next-generation waveform. *IEEE Wirel. Commun.* **28**, 136–144 (2021).
6. Hong, Y., Thaj, T., Viterbo, E. *Delay-Doppler Communications: Principles and Applications* (Academic Press, 2022).
7. Kollengode Ramachandran, M., Chockalingam, A. Mimo-OTFS in high-Doppler fading channels: signal detection and channel estimation. In *2018 IEEE Global Communications Conference (GLOBECOM)*, 206–212 (IEEE, 2018).
8. Raviteja, P., Phan, K. T. & Hong, Y. Embedded pilot-aided channel estimation for OTFS in delay-doppler channels. *IEEE Trans. Veh. Technol.* **68**, 4906–4917 (2019).
9. Shen, W., Dai, L., An, J., Fan, P. & Heath, R. W. Channel estimation for orthogonal time frequency space (OTFS) massive mimo. *IEEE Trans. Signal Process.* **67**, 4204–4217 (2019).
10. Zhao, L., Gao, W.-J. & Guo, W. Sparse Bayesian learning of delay-Doppler channel for OTFS system. *IEEE Commun. Lett.* **24**, 2766–2769 (2020).
11. Yang, L., Bian, X., Li, M., Rui, Y. Variable resolution coarse-to-fine channel estimation method in fractional Doppler scenarios for ZP-OTFS. In *IEEE Transactions on Vehicular Technology* 1–6 (IEEE, 2025).
12. Wang, Q., Liang, Y., Zhang, Z. & Fan, P. 2d off-grid decomposition and SBL combination for OTFS channel estimation. *IEEE Trans. Wirel. Commun.* **22**, 3084–3098 (2023).
13. Shan, Y., Shafie, A., Yuan, J. & Wang, F. Off-grid channel estimation for orthogonal delay-Doppler division multiplexing using grid refinement and adjustment. *IEEE Trans. Wirel. Commun.* **24**, 3590–3605 (2025).
14. Wei, Z., Yuan, W., Li, S., Yuan, J. & Ng, D. W. K. Off-grid channel estimation with sparse Bayesian learning for OTFS systems. *IEEE Trans. Wirel. Commun.* **21**, 7407–7426 (2022).
15. Shan, Y., Wang, F. & Hao, Y. Off-grid channel estimation using grid evolution in rectangular pulse-shaping OTFS system. In: *2023 IEEE International Conference on Communications Workshops (ICC Workshops)*, 295–300 (IEEE, 2023).
16. Shan, Y. et al. Off-grid channel estimation using grid evolution for OTFS systems. *IEEE Trans. Wirel. Commun.* **23**, 9549–9565 (2024).
17. Jitsumatsu, Y. 2d sinc interpolation-based fractional delay and Doppler estimation using time and frequency shifted Gaussian pulses. In: *2025 International Conference on Artificial Intelligence in Information and Communication (ICAIIC)*, pp. 0060–0065 (ICAIIC, 2025).
18. Zhang, K. et al. Radar sensing via OTFS signaling: A delay Doppler signal processing perspective. In: *ICC 2023 - IEEE International Conference on Communications*, 6429–6434 (IEEE, 2023).
19. Zhu, J., Liang, J. Low complexity parameter estimation approach for OTFS-based ISAC system. In: *2025 IEEE Wireless Communications and Networking Conference (WCNC)*, 1–6 (IEEE, 2025).
20. Gaudio, L., Kobayashi, M., Caire, G. & Colavolpe, G. On the effectiveness of OTFS for joint radar parameter estimation and communication. *IEEE Trans. Wirel. Commun.* **19**, 5951–5965 (2020).
21. Aboutanios, E. & Mulgrew, B. Iterative frequency estimation by interpolation on Fourier coefficients. *IEEE Trans. Signal Process.* **53**, 1237–1242 (2005).
22. Serbes, A. Fast and efficient sinusoidal frequency estimation by using the DFT coefficients. *IEEE Trans. Commun.* **67**, 2333–2342 (2019).
23. Liao, J.-R. & Lo, S. Analytical solutions for frequency estimators by interpolation of DFT coefficients. *Signal Process.* **100**, 93–100 (2014).
24. Serbes, A. & Qaraqe, K. A fast method for estimating frequencies of multiple sinusoidals. *IEEE Signal Process. Lett.* **27**, 386–390 (2020).
25. Solak, V., Aldirmaz-Colak, S. & Serbes, A. Fast and efficient 2-d and *k*-d DFT-based sinusoidal frequency estimation. *IEEE Trans. Signal Process.* **70**, 5087–5101 (2022).
26. Tse, D. & Viswanath, P. *Fundamentals of Wireless Communication* (Cambridge University Press, 2005).
27. Li, J. & Stoica, P. Efficient mixed-spectrum estimation with applications to target feature extraction. *IEEE Trans. Signal Process.* **44**, 281–295 (1996).
28. Rissanen, J. A universal prior for integers and estimation by minimum description length. *Ann. Stat.* **11**, 416–431 (1983).
29. Diao, R. & Meng, Q. An interpolation algorithm for discrete Fourier transforms of weighted damped sinusoidal signals. *IEEE Trans. Instrum. Meas.* **63**, 1505–1513 (2014).
30. Roy, R. & Kailath, T. Esprit-estimation of signal parameters via rotational invariance techniques. *IEEE Trans. Acoust., Speech, Signal Process.* **37**, 984–995 (1989).
31. Schmidt, R. Multiple emitter location and signal parameter estimation. *IEEE Trans. Antennas Propag.* **34**, 276–280 (1986).
32. ETSI. LTE; Evolved Universal Terrestrial Radio Access (E-UTRA); Relay radio transmission and reception. ETSI TS136 116, Version 18.1.0, Release 18 (Apr 2025). Available at https://www.etsi.org/deliver/etsi_ts/136100_136199/136116/18.01.00_60/ts_136116v180100p.pdf.
33. 3rd Generation Partnership Project (3GPP) NR; Multiplexing and channel coding. Technical Specification 3GPP TS 38.212, 3GPP Technical Specification Group Radio Access Network (April 2025). Release 18. https://www.etsi.org/deliver/etsi_ts/138200_138299/138212/18.06.00_60/ts_138212v180600p.pdf (2025).

Acknowledgements

This work was conducted within the MiFuture project, which has received funding from the European Union's Horizon Europe (HE) MarieSkłodowska-Curie Actions MiFuture HORIZON-MSCA2022-DN-01, under Grant Agreement number 101119643 and YAHYA/6G HORIZON-MSCA-2022-PF-01, under Grant Agreement number 101109435. The work was partially supported by Portuguese national funds through FCT – Fundação para a

Ciência e a Tecnologia, I.P., and, when eligible, co-funded by EU funds under project/support UID/50008/2025 – Instituto de Telecomunicações, with DOI identifier "https://doi.org/10.54499/UID/50008/2025".

Author contributions

Omid Abbassi Aghda led the writing and conducted the main simulations. Nikolajs Tihomorskis contributed to SDR-based simulations. Oussama Ben Haj Belkacem, Rui Dinis, João Guerreiro, Nuno Souto, and Michal Szczachor provided supervision, technical guidance, and support in algorithm development and validation. All authors contributed to reviewing, editing, and validating the results.

Competing interests

The authors declare no competing interests.

Additional information

Correspondence and requests for materials should be addressed to Omid Abbassi Aghda.

Reprints and permissions information is available at http://www.nature.com/reprints

Publisher's note Springer Nature remains neutral with regard to jurisdictional claims in published maps and institutional affiliations.

Open Access This article is licensed under a Creative Commons Attribution-NonCommercial-NoDerivatives 4.0 International License, which permits any non-commercial use, sharing, distribution and reproduction in any medium or format, as long as you give appropriate credit to the original author(s) and the source, provide a link to the Creative Commons licence, and indicate if you modified the licensed material. You do not have permission under this licence to share adapted material derived from this article or parts of it. The images or other third party material in this article are included in the article's Creative Commons licence, unless indicated otherwise in a credit line to the material. If material is not included in the article's Creative Commons licence and your intended use is not permitted by statutory regulation or exceeds the permitted use, you will need to obtain permission directly from the copyright holder. To view a copy of this licence, visit http://creativecommons.org/licenses/by-nc-nd/4.0/.

© The Author(s) 2026